

# Geometric and experimental models of extensional fault-bend folds

MARTHA O. WITHJACK & ROY W. SCHLISCHE

*Department of Geological Sciences, Rutgers University, Piscataway, New Jersey, 08854, USA*  
(e-mail: drmeow3@yahoo.com)

**Abstract:** We use geometric and experimental models to study the development of extensional fault-bend folds. The geometric models show that fault shape, fault displacement, and patterns of aggradation/erosion profoundly affect the distribution of growth beds, the magnitude and direction of dip of pregrowth and growth beds, and the location and dip of the outer limit of folding in pregrowth and growth beds. Complex structural and stratigraphic patterns develop if the rate of aggradation/erosion relative to the rate of fault displacement changes through time. The experimental models (with dry sand and wet clay) show that several deformational styles can accommodate extensional fault-bend folding. In sand models, a few, relatively major, secondary antithetic normal faults accommodate most hanging wall deformation. Pregrowth layers, although faulted, remain flat. The effective shear direction parallels the antithetic normal faults, and the shear angle is about  $60^{\circ}$ – $65^{\circ}$ . In clay models, numerous, relatively minor, secondary normal faults (antithetic and synthetic) and cataclastic flow accommodate most hanging wall deformation. The deformed pregrowth and growth layers dip gently toward the main fault. The effective shear angle ( $35^{\circ}$ – $50^{\circ}$ ) is considerably less than the dip of the antithetic normal faults. In the sand models and geometric models with a large shear angle ( $60^{\circ}$ ), more displacement occurs on the main normal fault and the hanging wall collapses in a relatively narrow zone. In the clay models and geometric models with a small shear angle ( $35^{\circ}$ ), less displacement occurs on the main normal fault. Instead, the hanging wall stretches substantially and collapses in a relatively wide zone.

Normal faults have a great variety of shapes in cross-sectional view. Some are listric (i.e., concave upward), either dipping (Fig. 1a) or flattening at depth (Figs 1b–d). Others steepen with depth (Fig. 1e). Still others have complex ramp-flat-ramp geometries (Fig. 1f). Movement on nonplanar normal faults causes the hanging wall to deform, typically by extensional fault-bend folding. Several researchers have used experimental and geometric models to study the development of extensional fault-bend folds. Experimental studies with wet clay (e.g., H. Cloos 1928, 1930; E. Cloos 1968; Withjack *et al.* 1995) and dry sand (e.g., McClay & Ellis 1987a, b; Ellis & McClay 1988; McClay & Scott 1991) have simulated the secondary faulting and folding associated with movement on nonplanar normal faults. Geometric studies (e.g., White *et al.* 1986; Dula 1991; White & Yielding 1991; Kerr & White 1992; Xiao & Suppe 1992; Withjack & Peterson 1993) have examined how fault shape, fault displacement and depositional patterns affect hanging wall geometries and tested the applicability of geometric modelling.

Each modelling approach has strengths and weaknesses. With geometric models, it is easy to vary fault shape, fault displacement and depositional/erosional patterns. It is necessary, however, to prescribe a hanging wall deformation mechanism, typically layer-parallel shear in compressional settings or inclined simple shear in extensional settings (Fig. 2). With experimental models, it is difficult to vary fault shape without imposing unrealistic boundary conditions (e.g., Withjack *et al.* 1995; Hauge & Gray 1996). The hanging wall, however, can deform by a range of deformation mechanisms that can vary spatially and temporally. In this paper, we use these complementary modelling approaches to better understand the development of extensional fault-bend folds. Specifically, we use the geometric models to document how fault shape, fault displacement, depositional and erosional patterns, and multiple episodes of faulting affect the geometry of extensional fault-bend folds. We use experimental models with dry sand and wet clay to study the hanging wall deformation that accommodates extensional fault-bend folding.

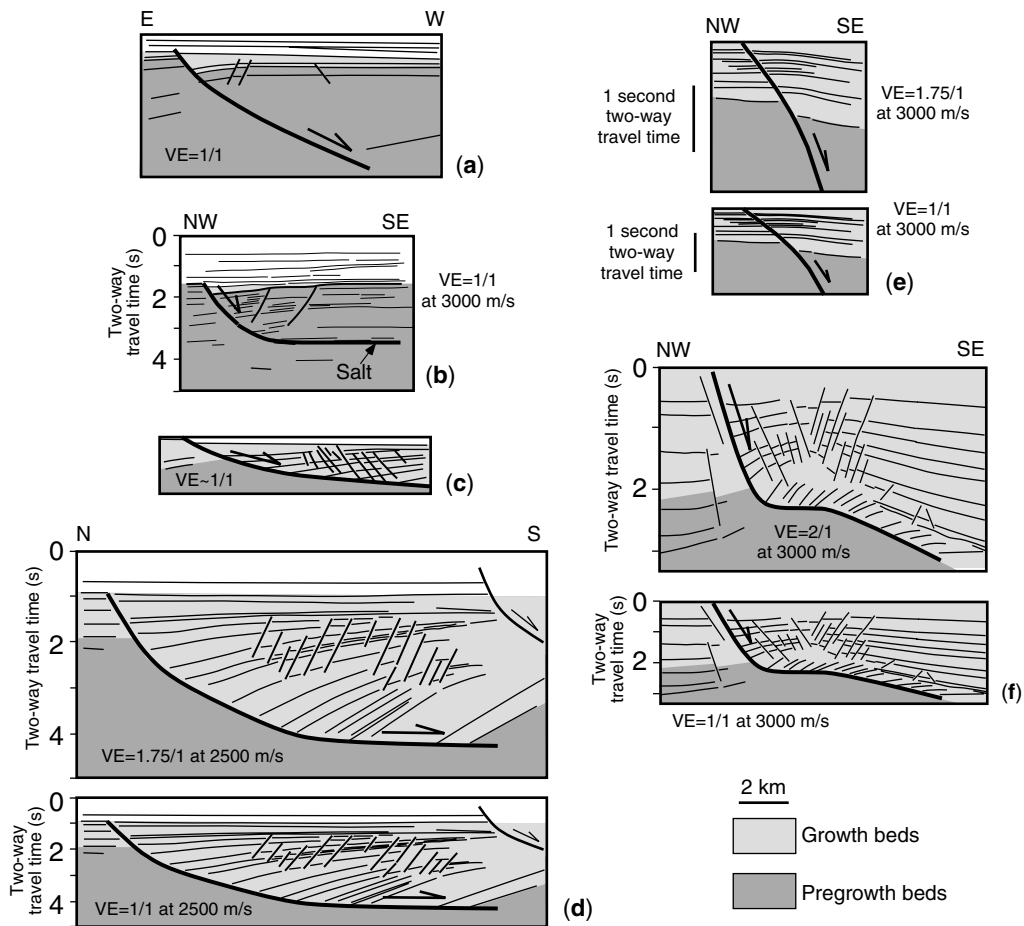


**Fig. 1.** Examples of normal faults and extensional fault-bend folds. (a) Line drawing of seismic line from offshore Norway (converted to depth) showing listric normal dipping at depth, rollover fold and secondary normal faults (Yielding *et al.* 1991). (b) Line drawing of migrated seismic line from offshore Norway showing listric normal fault flattening at depth in salt, rollover fold and antithetic secondary normal faults (after Withjack & Peterson 1990). (c) Line drawing of seismic line from Gulf of Oman with listric normal fault flattening at depth, rollover fold and synthetic secondary normal faults (after Wernicke & Burchfiel 1982; Hauge & Gray 1996). The line is displayed with approximately no vertical exaggeration. (d) Line drawing of migrated seismic line from Gulf of Mexico with listric normal fault flattening at depth, rollover fold and antithetic secondary normal faults. (e) Line drawing of migrated seismic line from offshore Australia (Northwest Shelf) showing normal fault that steepens with depth and associated hanging wall fold. (f) Line drawing of migrated seismic line from Gulf of Mexico showing normal fault (Brazos fault) with ramp-flat-ramp geometry, hanging wall folding, and complex pattern of secondary normal faulting. The line drawings in panels d-f are displayed with (top) and without (bottom) vertical exaggeration.

### Geometric modelling

Movement on a nonplanar fault surface creates a potential gap between the footwall and hanging wall (Fig. 2a). In our geometric models, we assume that deformation of the hanging wall by inclined simple shear closes this gap, forming an extensional fault-bend fold. Numerous case studies have shown that inclined simple shear

is a reasonable approximation of the bulk deformation in the hanging walls of nonplanar normal faults (e.g., White & Yielding 1991; Kerr & White 1992; White 1992; Xiao & Suppe 1992; Withjack & Peterson 1993; Withjack *et al.* 1995; Hauge & Gray 1996). For simplicity, we assume that the inclined shear direction dips  $70^\circ$  toward the main normal fault. We also assume that the footwall remains rigid, that

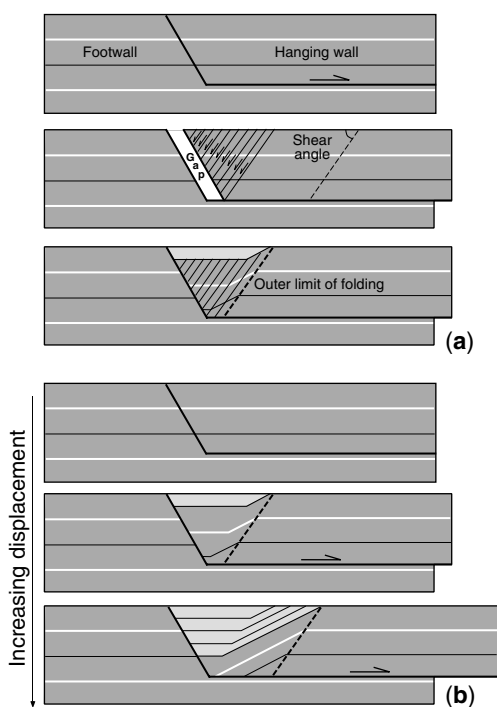


**Fig. 2.** Geometric modelling technique. (a) Movement on a nonplanar normal fault creates a potential gap between the footwall and hanging wall. Deformation of the hanging wall by inclined shear closes the gap and forms an extensional fault-bend fold. A growth bed fills the depression above the fold. (b) As fault displacement increases, fault-bend folding continues and new growth beds fill the resultant depressions above the fold. The pregrowth and growth beds deform as fault displacement increases.

compaction is negligible, and that growth beds completely fill any depressions that develop during faulting up to a prescribed regional datum (Fig. 2b). Although these factors certainly affect the geometry of extensional fault-bend folds (e.g., White & Yielding 1991; Xiao & Suppe 1992), the focus of this paper is to systematically study the effects of fault shape, fault displacement, and patterns of deposition and erosion for one or more episodes of normal faulting.

### Experimental modelling

In our experimental models, either dry sand or wet clay represents the sedimentary overburden. The dry sand is composed of quartz grains with diameters of less than 0.5 mm (Withjack & Callaway 2000). Its density is about  $1600 \text{ kg m}^{-3}$ .

It has a negligible cohesion, and a coefficient of internal friction of about 0.6. Localized cataclastic faulting (e.g., Rutter 1986) is the primary deformation style, even when strains are small. Thus, the dry sand has a negligible ductility as defined by Rutter (1986). The wet clay is composed predominantly of kaolinite and water (c. 40% by weight) (Withjack & Callaway 2000). Its density is about  $1600 \text{ kg m}^{-3}$ . It has a low cohesion (c. 50 Pa) and a coefficient of internal friction of about 0.5. Distributed cataclasis (e.g., Rutter 1986) is the primary deformation style in the wet clay when strains are small. With increasing strain, however, deformation becomes localized and cataclastic faulting is the primary deformation style. Thus, the wet clay has a greater ductility than that of the dry sand. The cohesion and coefficient of internal friction of the dry sand and wet clay are appropriate to ensure dynamic similarity between the models and natural prototypes (see Appendix). The sand and clay, however, simulate different types of rocks. The dry sand, with its negligible cohesion and ductility, represents rock that deforms primarily by localized cataclastic faulting (e.g., granite that deforms into large fault blocks with little internal deformation). The wet clay, with its greater cohesion and ductility, represents rock that deforms by distributed cataclasis and localized cataclastic faulting (e.g., interbedded sandstone and shale that deforms into fault blocks with considerable internal deformation).

Our experimental models have two different set-ups. One set-up has two overlapping metal plates beneath a 4 cm-thick layer of dry sand or wet clay (Fig. 3a). During the experiments, the lower plate slides outward at  $4 \text{ cm hr}^{-1}$ . In response, a normal fault propagates upward from the edge of the fixed, upper plate through the overlying sand or clay layer. The second set-up, originally described in Withjack and Callaway (2000), has two juxtaposed metal blocks beneath a 4 cm-thick layer of dry sand or wet clay (Fig. 3b). The  $45^\circ$ -dipping boundary between the metal blocks represents a dipping normal fault. During the experiments, the hanging wall block slides down the normal fault at  $0.25 \text{ cm hr}^{-1}$ . In response, a normal fault propagates upward from the edge of the footwall block through the overlying sand or clay layer. During the experiments, we fill subsiding areas with either dry sand or wet clay to simulate deposition during deformation. Also, we photograph the top surface of the models to document the surface deformation through time. After the experiments, we vertically slice the models, creating serial cross sections that

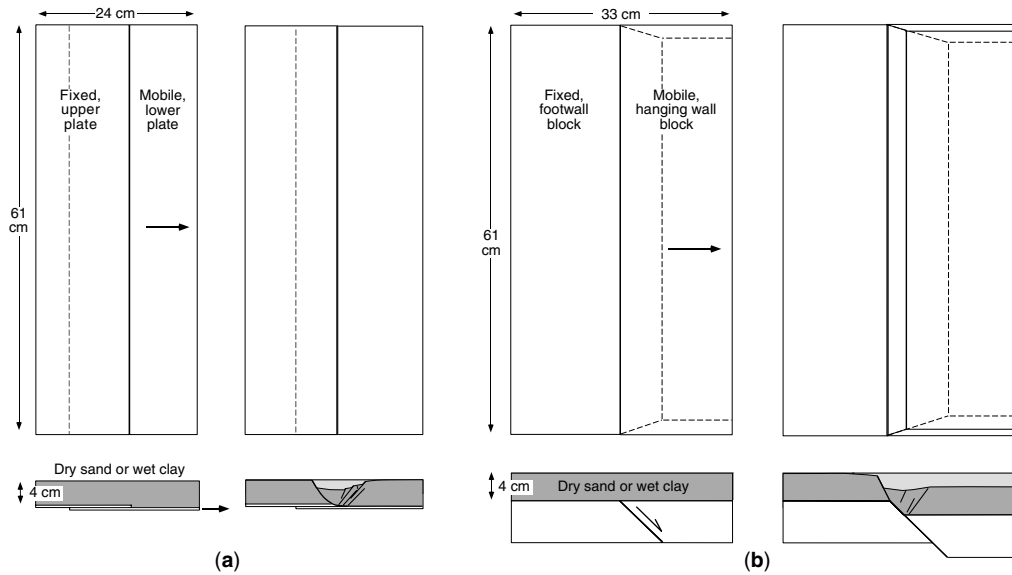


**Fig. 3.** Experimental modelling technique. (a) Experimental set-up with two overlapping metal plates beneath a layer of dry sand or wet clay. During the experiments, the lower plate slides away from the upper plate. (b) Experimental setup with two juxtaposed metal blocks beneath a layer of dry sand or wet clay. The  $45^\circ$ -dipping boundary between the blocks represents a dipping normal fault. During the experiments, the hanging wall block slides downward.

record the final deformation throughout the models. Colored (but mechanically identical) sub-layers within the sand and clay help identify faults and folds.

## Results of geometric modelling

### *Fault shape*

Our geometric models, like those of White *et al.* (1986), Dula (1991), White and Yielding (1991), Kerr and White (1992), Xiao and Suppe (1992) and Withjack and Peterson (1993), show that fault shape profoundly affects the shape of an extensional fault-bend fold.

If a normal fault flattens/detaches at depth (Fig. 4, left column), then growth beds have a limited lateral distribution, provided no aggradation occurs during faulting. Far from the fault, pregrowth beds in the hanging wall rise to the level of their footwall counterparts. If the upper fault segment is planar (Fig. 4a), then a triangular panel of undeformed, flat-lying beds exists near the fault. Adjacent to this triangular panel, the deformed pregrowth and growth beds dip uniformly toward the normal fault. If the upper fault segment is listric (Fig. 4b), then pregrowth and growth beds dip toward the fault. The dip of

the growth beds systematically increases with depth, creating a fanning geometry.

If a normal fault dips at depth (Fig. 4, right column), then growth beds have a wide lateral distribution. All hanging wall beds are below the level of their footwall counterparts. The outer limit of the folding in the growth beds parallels the lowest fault segment, provided no aggradation or erosion occurs during faulting. If the upper fault segment is planar, then a triangular panel of undeformed, flat-lying beds exists near the fault. If the planar segment dips more steeply than the lower fault segment (Fig. 4c), then the tilted pregrowth and growth beds dip uniformly toward the main normal fault. If the planar segment dips more gently than the lower fault segment (Fig. 4d), then the tilted pregrowth and growth beds dip uniformly away from the main normal fault. If the upper fault segment is concave-upward (Fig. 4e), then the pregrowth and growth beds near the fault dip toward the fault. The dip of the growth beds systematically increases with depth, creating a fanning geometry. If the upper fault segment is convex-upward (Fig. 4f), then the pregrowth and growth beds near the fault dip away from the fault. Dips systematically increase

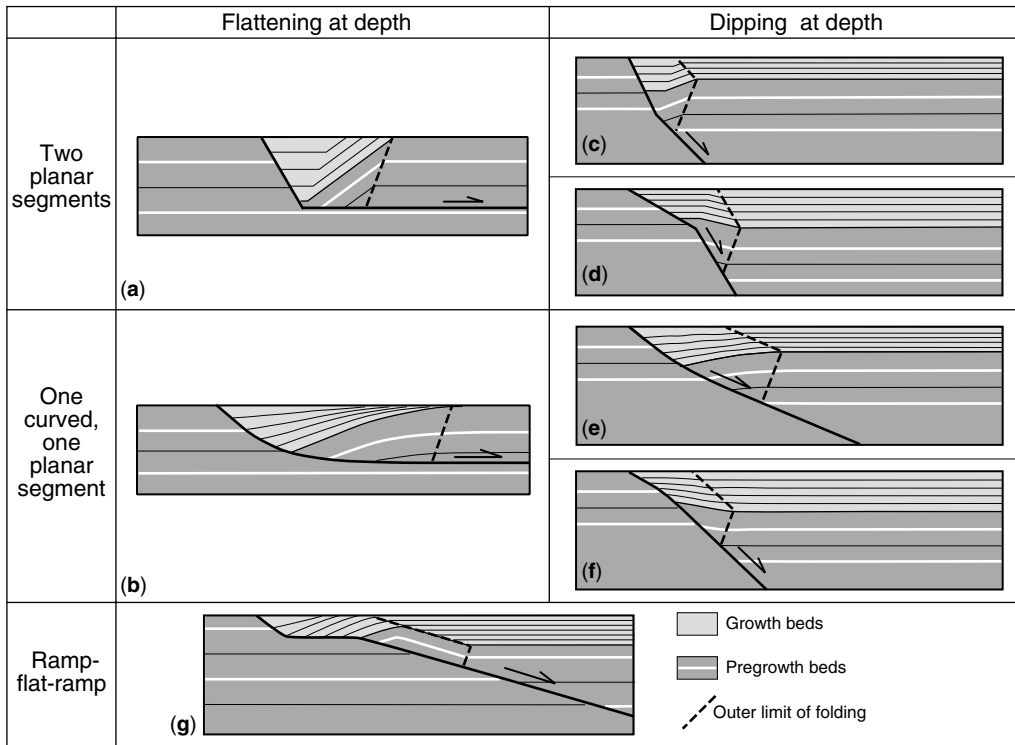


**Fig. 4.** Geometric models showing the effect of fault shape on the geometry of an extensional fault-bend fold. No aggradation or erosion occurs during faulting. Fault shape affects the lateral distribution of growth beds and the direction and magnitude of bedding dip. See text for further discussion.

with depth. This latter type of extensional fault-bend fold resembles a fault-propagation fold or a compaction-related fold.

If a normal fault has a ramp-flat-ramp geometry (Fig. 4g), then an anticline develops in the pre-growth beds. Growth beds near the fault dip and thicken toward the fault. Growth beds far from the fault are flat-lying. The outer limit of the folding in the growth beds parallels the lower ramp, provided no aggradation or erosion occurs during faulting.

*Fault displacement and fold evolution*

The geometry of an extensional fault-bend fold changes through time as fault displacement increases. If a fault has two planar segments (Fig. 2b), then fault displacement affects the distribution, but not the dip, of the deformed pre-growth and growth beds. As displacement increases, more of the pre-growth and growth beds deform. The dip of the deformed pre-growth and growth beds, however, remains constant. For a listric normal fault that flattens at depth

(Fig. 5a), the dip of the pre-growth beds increases as fault displacement increases. Growth beds develop a pronounced fanning geometry, and pre-growth and growth beds become thinner and longer. When fault displacements are very large, the oldest growth beds are substantially thinned and lengthened. Their fanning geometry becomes subtle, making it difficult to distinguish between growth and pre-growth layers.

For a normal fault with a ramp-flat-ramp geometry (Fig. 5b), a wide anticline initially forms in the pre-growth beds above the flat. Near the fault, growth beds dip and thicken toward the fault. Far from the fault, growth beds are flat-lying. No deposition occurs above the central part of the flat across the crest of the anticline. As fault displacement increases, the anticline narrows and moves down the lower ramp. Growth beds continue to accumulate near and far from the fault, but not above the central part of the flat. With additional fault displacement, the site of no deposition moves down the lower ramp, producing a dipping, diachronous unconformity. Correlative beds are offset across

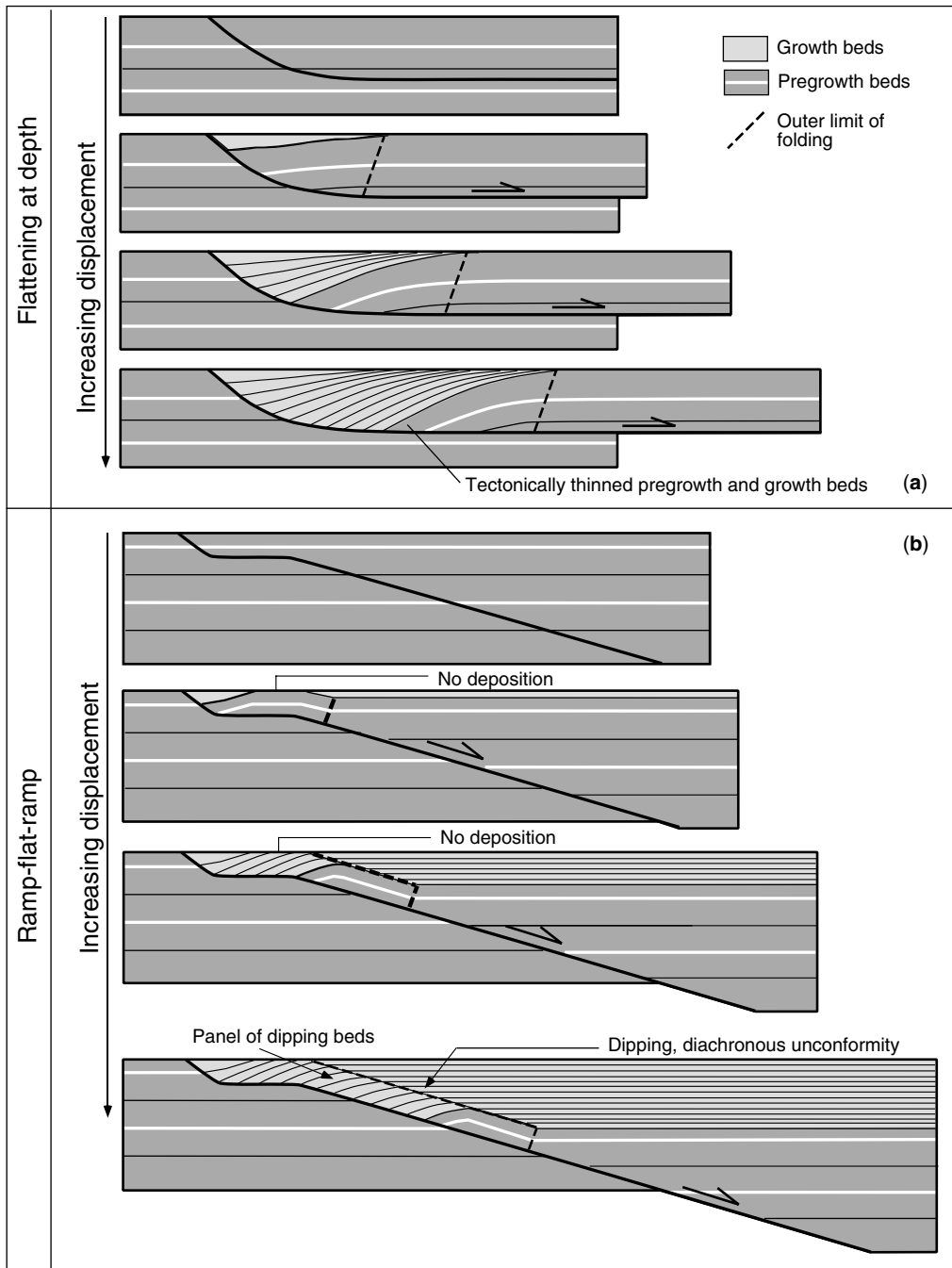


**Fig. 5.** Geometric models showing the effect of fault displacement on the geometry and evolution of an extensional fault-bend fold. No aggradation or erosion occurs during faulting. (a) Listric fault that flattens at depth. (b) Fault with ramp-flat-ramp geometry. See text for further discussion.

the unconformity. Thus, the unconformity resembles a normal fault that parallels the lower ramp. A panel of dipping growth beds develops directly above the lower ramp.

*Aggradation and erosion*

In many extensional settings, regional subsidence, regional uplift, and fluctuations in sediment supply or sea level lead to aggradation or erosion during normal faulting. Our geometric models (Figs 6 and 7) support the conclusion of Xiao and Suppe (1992) that the rate of aggradation relative to the rate of fault displacement profoundly affects the shape of an extensional fault-bend fold. Additionally, our geometric models show that the rate of erosion relative to the rate of fault displacement also profoundly affects the shape of an extensional fault-bend fold.

For a listric fault that flattens at depth (Fig. 6a), growth beds have a wide lateral distribution

with aggradation and a very limited lateral distribution with erosion. With erosion, growth beds have a more subtle fanning geometry and can, in fact, closely resemble pregrowth beds. For a fault that dips at depth (Fig. 6b), the dip of the outer limit of the folding in the growth beds depends on the amount of aggradation or erosion that occurs during faulting. As mentioned previously, the outer limit of the folding in the growth beds parallels the lower fault segment, if no aggradation or erosion occurs (Fig. 4). With aggradation, the outer limit of the folding dips more steeply than the lower fault segment. The greater the amount of aggradation, the steeper the dip. With erosion, the outer limit of the folding dips more gently than the lower fault segment. The greater the amount of erosion, the gentler the dip. For a normal fault with a ramp-flat-ramp geometry (Fig. 7), a panel of dipping growth beds develops above the lower ramp with aggradation and with

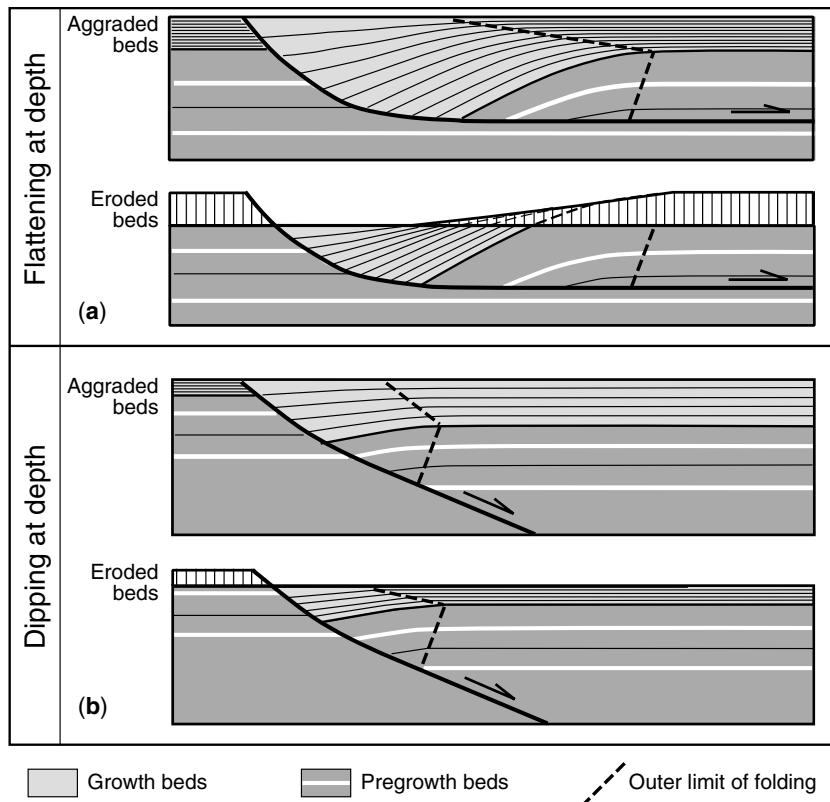


**Fig. 6.** Geometric models showing the effect of aggradation and erosion on the geometry of an extensional fault-bend fold. (a) Fault that flattens at depth. (b) Fault that dips at depth. The occurrence of aggradation/erosion affects the lateral distribution of growth beds, the dip of the growth beds, and the outer limit of the folding. See text for further discussion.

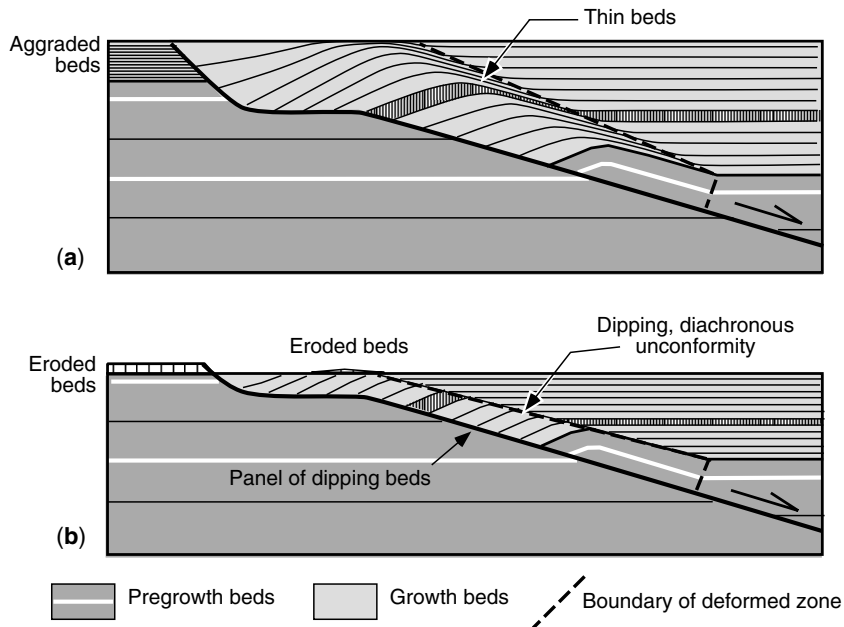


**Fig. 7.** Geometric models of faults with ramp-flat-ramp geometry showing the effect of (a) aggradation and (b) erosion on the geometry of an extensional fault-bend fold. The occurrence of aggradation/erosion affects the lateral distribution of growth beds, the dip of the growth beds, and the outer limit of the folding. See text for further discussion.

erosion. With aggradation, the panel widens upward, and thin growth beds dipping away from the fault overlie the panel (Fig. 7a). With erosion, the panel narrows upward, and a dipping, diachronous unconformity overlies the panel. The unconformity dips more gently than the lower ramp (Fig. 7b).

#### *Multiple episodes of faulting*

Complex structural and stratigraphic patterns develop with multiple episodes of normal faulting if the rate of aggradation/erosion relative to the rate of fault displacement changes through time (Fig. 8). In Figures 8a–c, the normal fault is listric and flattens at depth. In Figure 8a, aggradation occurs during the second episode of faulting but not during the first episode. The distribution and geometry of the growth beds associated with each faulting episode differ substantially. The outer limit of the folding is not planar. It parallels the inclined shear direction in the pre-growth beds, it flattens above the growth beds associated with the first faulting episode, and it dips away from the fault in the growth beds associated with the second faulting episode. In Figure 8b, widespread deposition occurs between episodes of normal faulting. The outer

limit of the folding parallels the inclined shear direction in the pre-growth beds. It flattens above the growth beds associated with the first faulting episode, and it parallels the inclined shear direction in the beds deposited between the faulting episodes. In Figure 8c, erosion occurs between the episodes of normal faulting. The growth beds associated with the first faulting episode have a very subtle fanning geometry. In fact, they closely resemble the underlying pre-growth beds. In Figure 8d, the normal fault has a ramp-flat-ramp geometry. If significant aggradation occurs during the second episode of faulting but not during the first episode, then the distribution and geometry of the growth beds associated with each faulting episode differ substantially. The outer limit of the folding is not planar. It parallels the lower ramp in the growth beds associated with the first faulting episode, and it dips toward the fault in the growth beds associated with the second faulting episode.

#### **Results of experimental modelling**

As discussed below, the sand and clay models provide information about the styles of deformation associated with extensional fault-bend folding (Figs 9–11).

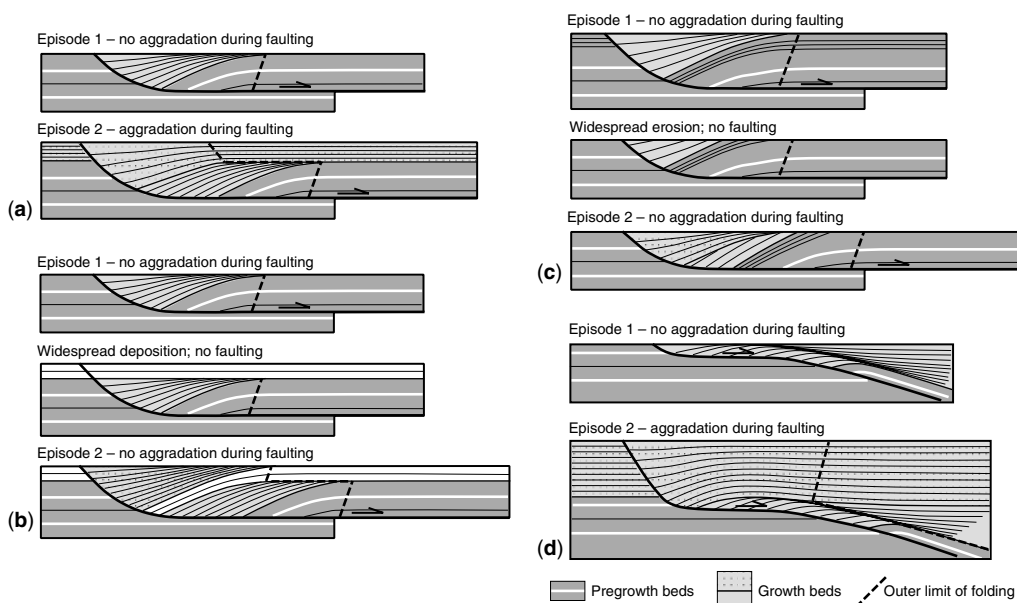


**Fig. 8.** Geometric models showing the effect of multiple episodes of faulting on the geometry of an extensional fault-bend fold. The rates of aggradation/erosion relative to the rates of fault displacement vary during the faulting episodes. See text for further discussion.

*Models with overlapping plates: horizontal detachment at depth*

In the sand model with the overlapping plates (Fig. 9a), a fault propagates upward from the edge of the fixed upper plate. The fault is planar and dips steeply, about 60°–65°. This steep fault and the horizontal mobile plate, together represent a normal fault that flattens/detaches at depth. A fault bend separates the steep and horizontal segments. As the deformation progresses, a series of steeply dipping antithetic faults develops in the hanging wall. Each antithetic fault forms near the fault bend, moves with the mobile plate past the fault bend, and becomes inactive. Thus, the antithetic faults become progressively older the farther from the fault bend. The antithetic faults have relatively large displacements and accommodate most of the hanging wall deformation, accounting for about 40% of the imposed displacement of the mobile plate (Fig. 9c). The upper segment of the main normal fault accounts for another 45% of the imposed displacement. The remainder (15%) is internal deformation within the fault blocks. Kautz and Sclater (1988) determined similar amounts of internal deformation in their extensional sand models. The effective shear direction in the sand model

(based on the outer limit of the folding) is sub-parallel to the antithetic normal faults. Thus, the inclined shear angle in the sand model is about 60°–65°, agreeing with the value obtained by Xiao and Suppe (1992) for a similar sand model published by McClay and Ellis (1987a).

In the clay models with the overlapping plates (Figs 9b and 11a–d), a fault propagates upward from the edge of the fixed upper plate. Unlike the sand models, fault-propagation folding and secondary faulting precede the development of the through-going normal fault. The fault is listric, steeply dipping (*c.* 75°) near the surface and gently dipping (*c.* 35°) near the base of the clay layer. This steep fault and the horizontal mobile plate, together, represent a normal fault that flattens/detaches at depth. A fault bend separates the steep and horizontal segments. As displacement increases, an upward-widening zone of deformation develops, emanating from the fault bend (Fig. 11a). Deformation includes secondary normal faulting (antithetic and synthetic) and fault-bend folding (layers dip toward the main normal fault). The deformation zone moves with the mobile plate, passing the fault bend. Eventually, it becomes inactive and a new deformation zone replaces it (Figs 11b, c). Thus, deformation becomes progressively older

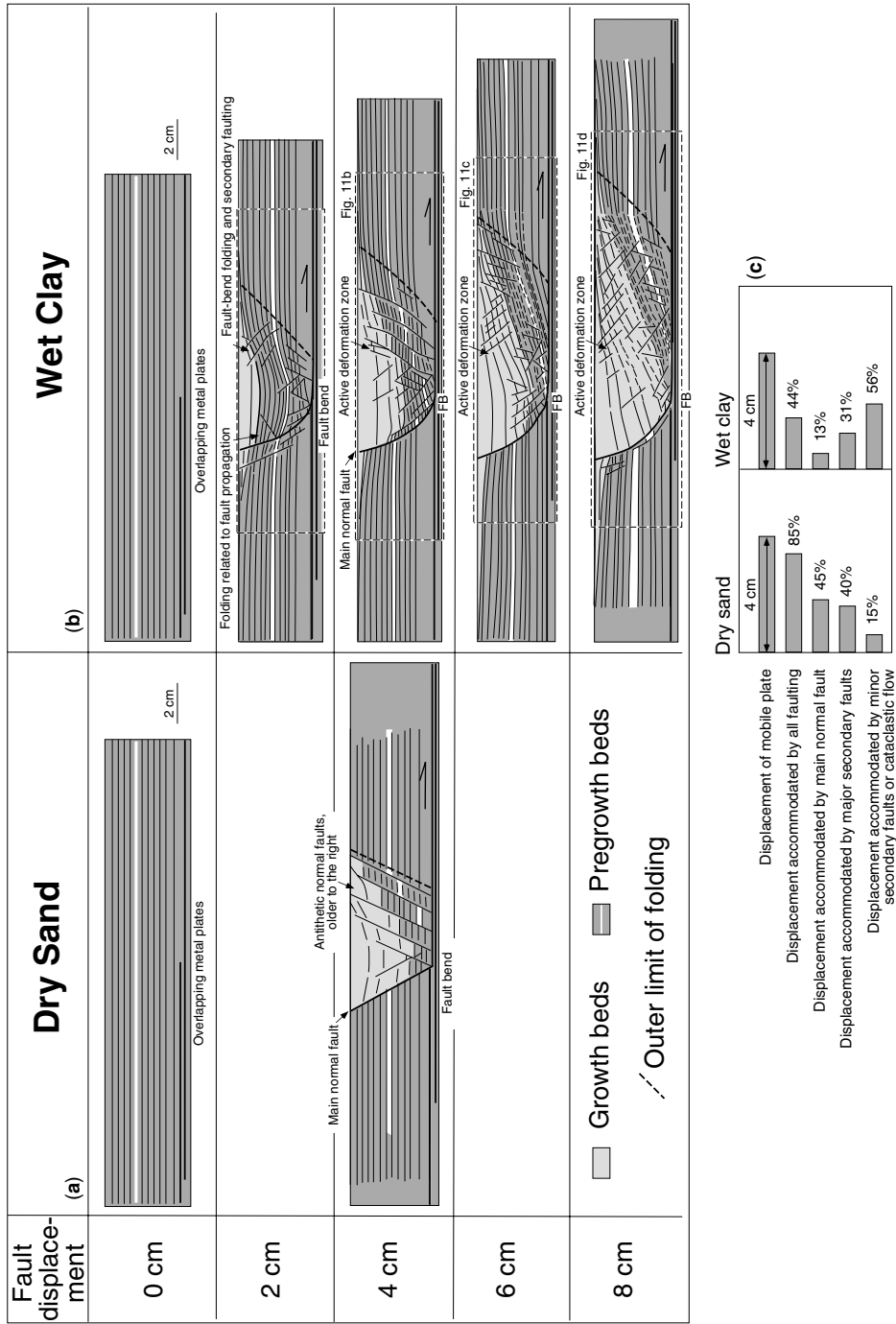


**Fig. 9.** Line drawings of cross sections through (a) experimental models with dry sand and (b) four experimental models with wet clay. The sand or clay layer overlies overlapping metal plates. During the experiments, the lower plate moves to the right by a prescribed displacement. The experimental models simulate fault-bend folding associated with a normal fault that flattens at depth. The boxes show the locations of the photographs in Fig. 11. FB is fault bend (c) Accommodation of imposed displacement (4 cm) in the sand and clay models.

the farther from the fault bend. By 8 cm of displacement of the mobile plate (Fig. 11d), most pregrowth and growth layers are faulted and dip gently (*c.* 20°) toward the main fault. Fault-bend folding rotates many of the secondary faults. Thus, synthetic faults dip more gently and antithetic faults dip more steeply through time. The pregrowth beds and the oldest growth beds have thinned and lengthened significantly. In fact, many of the oldest growth beds lack an obvious fanning geometry and resemble pregrowth beds (Fig. 11d).

In the clay models, cataclastic faulting, cataclastic flow and rigid-body rotation accommodate the fault-bend folding. For example, in the model with 4 cm of displacement of the mobile plate, the major secondary faults account for about 31% of the imposed displacement (Fig. 9c). The upper segment of the main normal fault accounts for another 13% of the imposed displacement. Minor faulting, cataclastic flow, and rigid-body rotation account for 56% of the imposed displacement. Kautz and Sclater (1988) determined similar amounts of internal deformation within their extensional clay models. The effective shear angle is about 35°–50° (based on the average dip of the outer limit of the folding), considerably less than the dip of the antithetic faults. White and Yielding (1991) calculated a similar value (49°) for a published clay model by E. Cloos (1968), and Withjack *et al.* (1995) obtained similar values (50°–55°) for their clay-model experiments.

#### *Models with juxtaposed blocks: dipping fault at depth*

In the sand model with the juxtaposed blocks (Withjack & Callaway 2000), a normal fault propagates upward from the edge of the fixed block (Fig. 10a). It is planar, and dips steeply, about 65°. This steep fault segment and the 45°-dipping boundary between the juxtaposed blocks represent a normal fault that dips at depth. A steeply dipping antithetic fault forms near the fault bend between the fault segments. It moves downward with the mobile block as fault displacement increases. Pregrowth and growth layers near the main fault dip gently toward the fault. The effective shear direction in the sand model (based on the dip of the outer limit of the folding) is subparallel to the antithetic normal fault. Thus, the inclined shear angle is about 65°.

In the clay model with the juxtaposed blocks (Withjack & Callaway 2000), a normal fault

propagates upward from the edge of the fixed block (Figs 10b and 11e). Fault-propagation folding and secondary faulting precede the development of the through-going normal fault. The fault is listric, steeply dipping (*c.* 90°) near the surface and gently dipping (*c.* 45°) near the base of the clay layer. This fault segment and the 45°-dipping boundary between the juxtaposed blocks represent a normal fault that dips at depth. An upward-widening zone of deformation develops in the hanging wall of the main normal fault. The zone, emanating from the fault bend, moves downward with the mobile block as fault displacement increases. Deformation within the zone includes secondary faulting (mostly antithetic normal faults) and fault-bend folding with pregrowth and growth layers dipping gently toward the main fault. The effective shear angle (based on the average dip of the outer limit of the folding in the pregrowth layers) is about 50°.

## Discussion and applications

### *Comparisons of geometric and experimental models*

The style of hanging wall deformation varies considerably in the experimental models, reflecting the differences in the cohesion and ductility of the dry sand and wet clay. In the sand models, a few, relatively large, secondary antithetic normal faults accommodate most of the hanging wall deformation. Pregrowth layers, although faulted, are flat-lying. The effective shear direction parallels the antithetic normal faults, and the shear angle is about 60°–65°. In the clay models, secondary faulting (antithetic and synthetic) and cataclastic flow accommodate most of the hanging wall deformation. The deformed pregrowth and growth layers dip gently toward the main normal fault. The effective shear angle (35°–50°) is considerably less than the dip of the antithetic normal faults.

The style of deformation in the sand models differs from that in the geometric models in several ways. Deformation is focused on a few, relatively large, antithetic normal faults in the sand models, not uniformly distributed as it is in the geometric models. Pregrowth layers are nearly flat-lying in the sand models, not dipping as they are in the geometric models. Although the distributed style of deformation in the clay models is similar to that in the geometric models, the clay models also differ from the geometric models in several ways. Fault-propagation folding precedes the development of through-going normal faults in

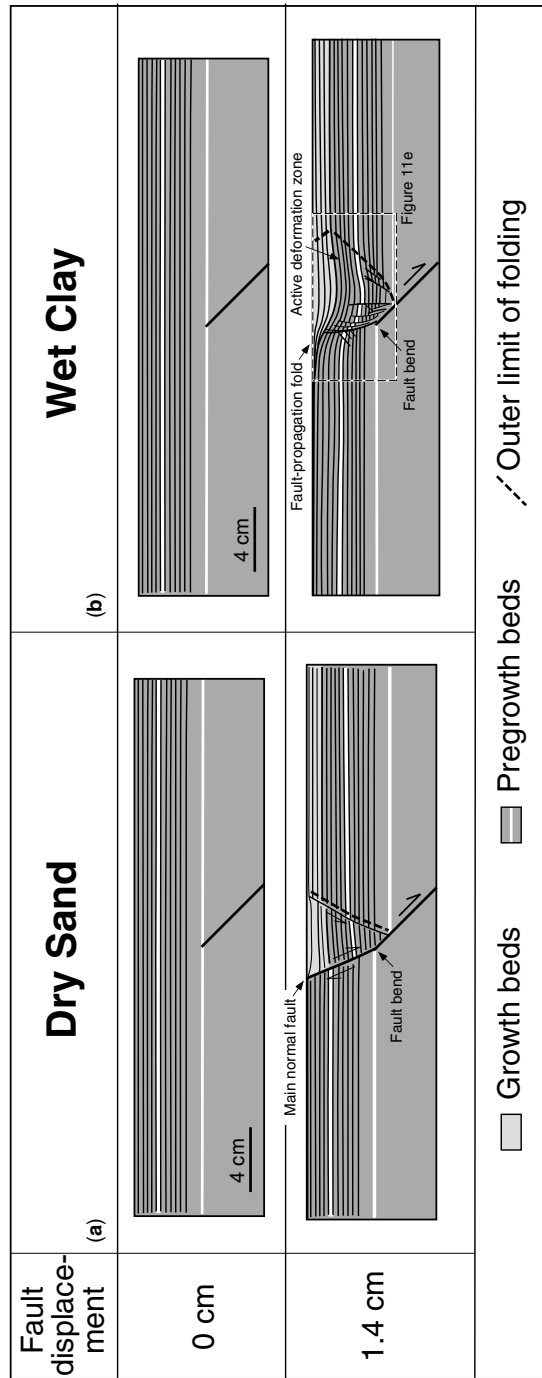


**Fig. 10.** Line drawings of cross sections through experimental models with dry sand and wet clay (after Withjack & Callaway 2000). The sand or clay layer overlies juxtaposed metal blocks. During the experiments, the hanging wall block moves downward by a prescribed displacement. The experimental models simulate fault-bend folding associated with a normal fault that dips at depth. The box shows the location of the photograph in Fig. 11e.

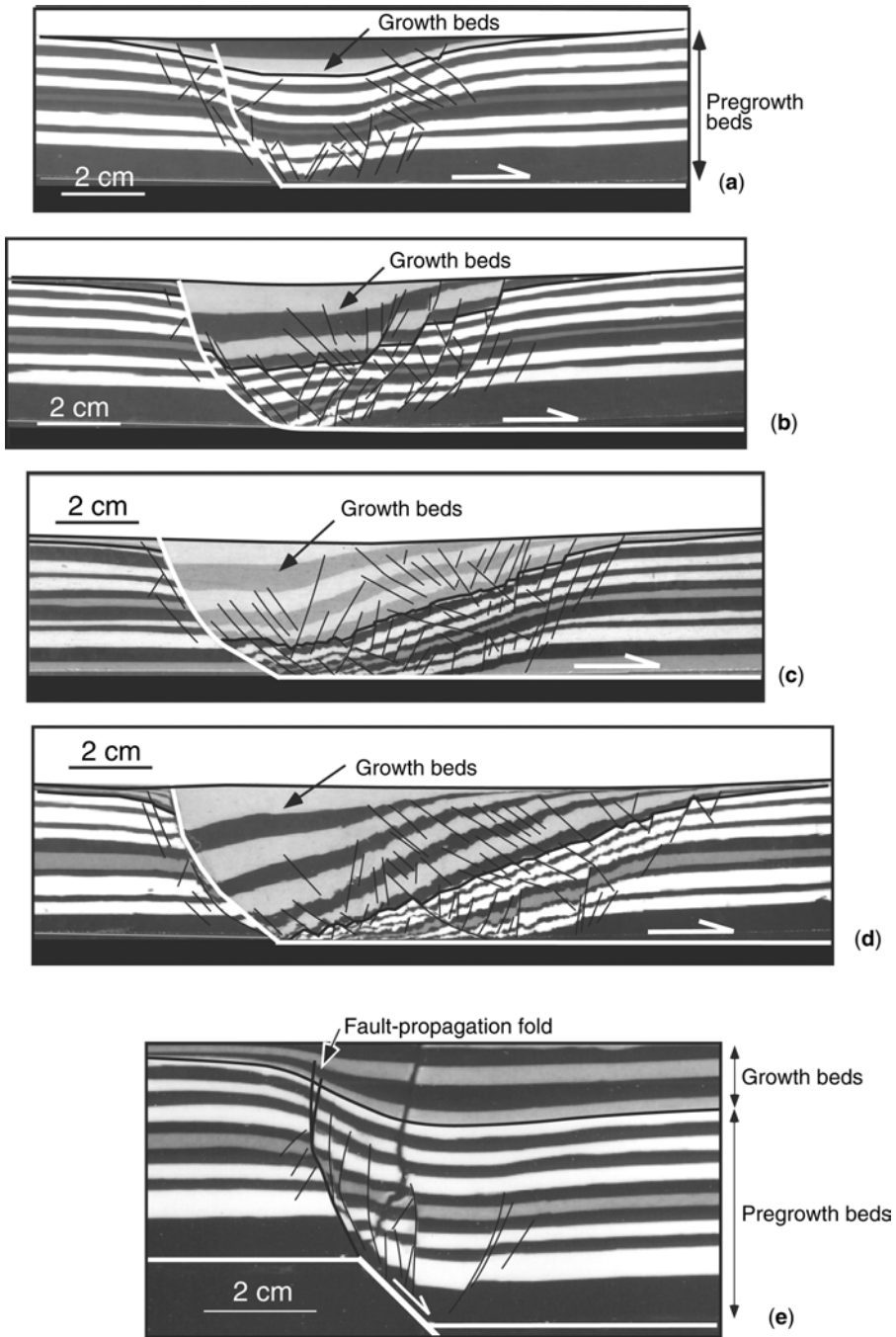


**Fig. 11.** Photographs of cross sections through five clay models. Major secondary faults are shown in black. (a) Cross section through model with 2 cm displacement of mobile plate. (b) Cross section through model with 4 cm displacement of mobile plate. (c) Cross section through model with 6 cm displacement of mobile plate. (d) Cross section through model with 8 cm displacement of mobile plate. (e) Cross section through model with 1.4 cm of displacement on mobile block.

the clay models. Thus, not all deformation in the clay models is related to fault-bend folding. Also, deformation zones in the pregrowth layers widen upward in the clay models. In geometric models with inclined shear, the width of the deformation zones in the pregrowth layers remains constant with depth (Withjack *et al.* 1995).

Despite differences in the styles of deformation, the geometric and experimental modelling approaches yield similar results for the overall shape and evolution of an extensional fault-bend fold. Specifically, in models with a normal fault that flattens at depth, growth beds have a limited lateral distribution. In models with a normal fault that dips at depth, growth beds have a wide lateral distribution. Both the geometric and experimental models show that rollover folds develop in the hanging walls of normal faults whose dip decreases with depth. The geometric and clay models with a listric, upper fault segment show that the dip of the growth beds increases with depth, creating a fanning geometry. If fault displacements are large, then pregrowth and growth beds thin and lengthen significantly during extensional fault-bend folding.

Figure 12 compares sand and clay models (with 4 cm of displacement of the mobile plate) with similar geometric models with shear angles of 60° and 35°, respectively. The distribution of deformation in the experimental models closely resembles that in the geometric models. In the sand model and the geometric model with the 60° shear angle, more displacement occurs on the upper segment of the main normal fault than in the clay model and the geometric model with the 35° shear angle. The hanging wall collapses in a relatively narrow zone in the sand model and the geometric model with the 60° shear angle. The hanging wall stretches substantially and collapses in a relatively wide zone in the clay model and the geometric model with the 35° shear angle.

Figure 13 compares a geometric model with a shear angle of 35° with the cross section from the clay model with 8 cm of displacement of the mobile plate. The clay model closely resembles the geometric model. Specifically, the location of the hanging wall cutoffs, the dip of the deformed hanging wall beds (*c.* 20°), and the displacement distribution for the pregrowth and growth beds are similar in both models. In the clay model and the geometric model, the hanging wall stretches considerably, requiring less displacement on the upper segment of the main normal fault. In the clay model, the youngest growth beds near the main normal fault dip and thicken toward the fault. In the geometric

model, the growth beds near the main normal fault are flat-lying. This difference reflects the listric shape of the upper fault segment in the clay model and the planar shape of the upper fault segment in the geometric model.

### *Geological examples*

Observed hanging wall folds in many natural examples resemble those in the geometric and experimental models. Rollover folds develop in the hanging wall of normal faults that flatten at depth (Figs 1b, c and d). Growth beds dip and thicken toward the main fault, and the oldest growth beds commonly have subtle fanning geometries. Normal faults with convex-up bends (Fig. 1e) have hanging wall beds that dip away from the main fault. Normal faults with ramp-flat-ramp geometries (Fig. 1f) have complex hanging wall deformation. Beds dip toward the fault near the main fault, and a dipping unconformity that parallels the lower ramp commonly develops above the ramp. The secondary normal faults in many natural examples resemble those in the experimental models. Many secondary normal faults are antithetic to the main fault (Figs 1a, b and d). Some, however, are synthetic to the main normal fault (Fig. 1c), like those in the clay models (Figs 9b and 11). Most secondary normal faults have relatively small displacements (Figs 1, 14 and 15), like those in the clay models (Figs 9b and 11). Calculated inclined shear angles for geological examples of extensional fault-bend folds (Hauge & Gray 1996) range from about 45°–70°, similar to those in the experimental models.

The Blackberry fault from the Gulf of Mexico (Fig. 14) has up to 10 km of normal displacement. It is listric, flattening within shales. Two small fault bends are present at shallow levels. Secondary normal faults in the hanging wall are antithetic to the Blackberry fault and have relatively small displacements. As predicted by the geometric and experimental models, a large rollover fold affects its hanging wall. Growth beds dip and thicken toward the fault. Second-order fault-bend folding occurs near the small fault bends. This folding, with beds dipping away from the Blackberry fault, resembles fault-propagation folding. It is, however, associated with beds passing through a convex-upward fault bend. Similar second-order fault-bend folds develop in our clay models (Fig. 14d). Xiao and Suppe (1992) have reported similar folds elsewhere in the Gulf of Mexico.

The Brazos fault from the Gulf of Mexico (Fig. 15) has two major fault bends, a northwest

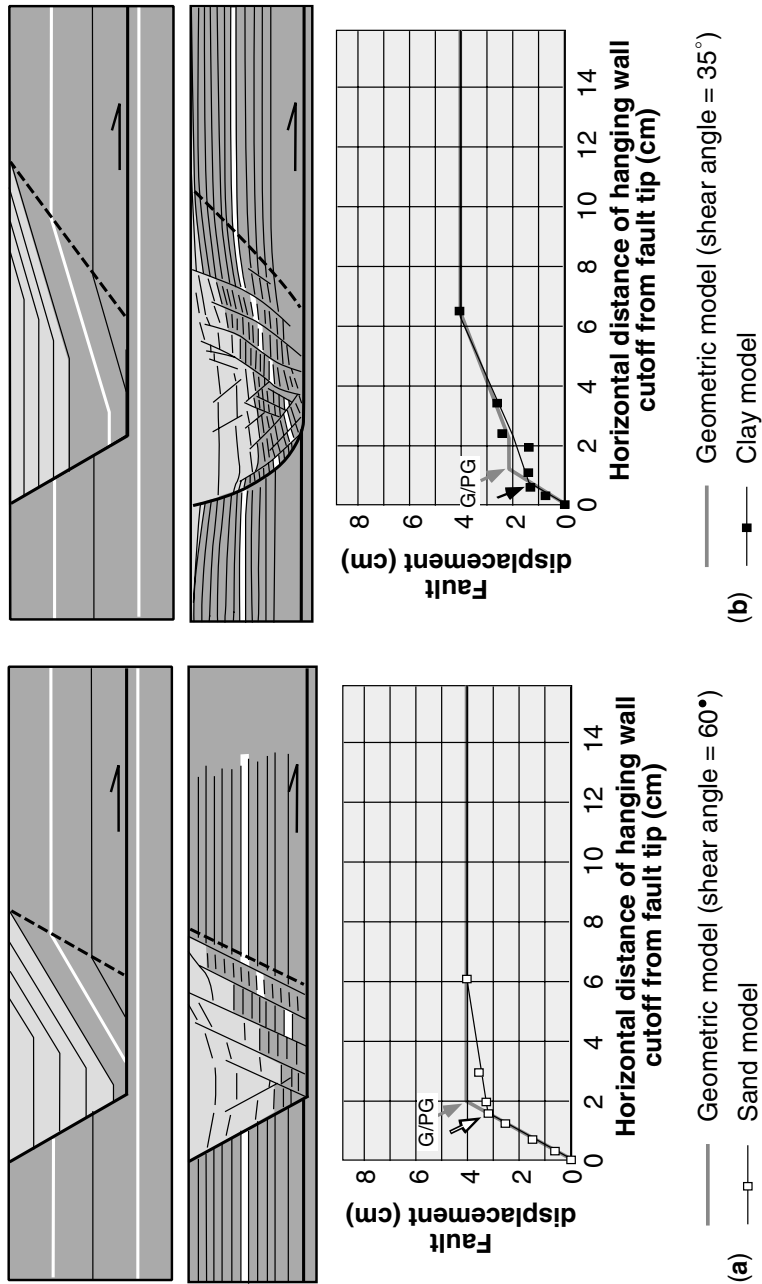


**Fig. 12.** (a) Line drawing of sand model (4 cm displacement of the mobile plate) and geometric model with 4 units of displacement and inclined shear angle of 60°. Plot of fault displacement versus horizontal distance of hanging wall cutoffs from fault tip for sand model and geometric model. (b) Line drawing of clay model (4 cm displacement of the mobile plate) and geometric model with 4 units of displacement and inclined shear angle of 35°. Plot of fault displacement versus horizontal distance of hanging wall cutoffs from fault tip for clay model and geometric model. G/PG indicates the boundary between the growth and pre-growth beds.

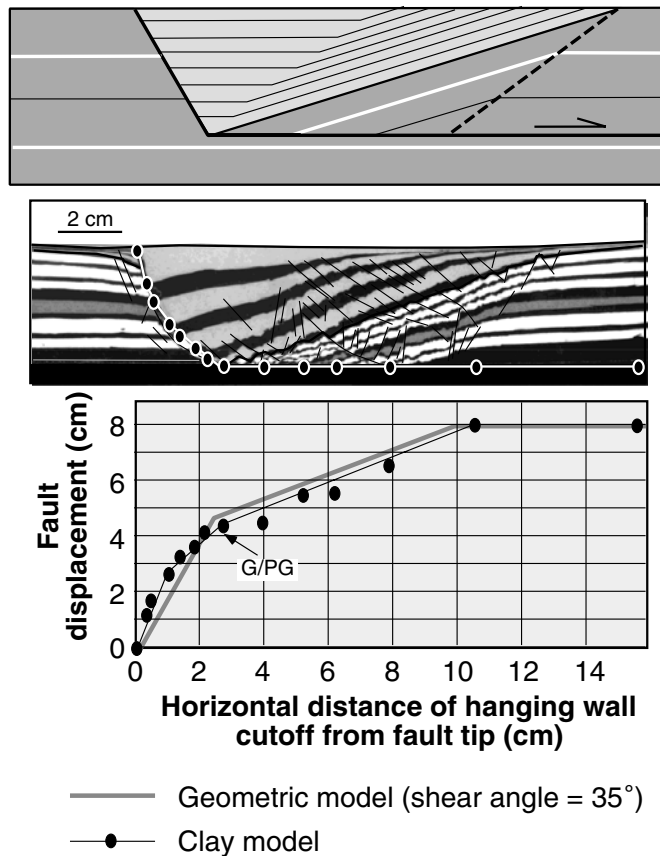


**Fig. 13.** Geometric model of fault-bend fold with 8 units of displacement (top). Inclined shear angle is  $35^\circ$ . Photograph of cross section of clay model after 8 cm of displacement (centre). Circles show locations of hanging wall cutoffs for key growth and pregrowth beds. Plot of fault displacement versus horizontal distance of hanging wall cutoffs from fault tip for clay model and geometric model (bottom). G/PG indicates the boundary between the growth and pregrowth beds.

concave-up bend and a southeast convex-up bend. The geometry of the fault changes considerably along strike (Vogler & Robinson 1987). On parts of the Brazos fault, the segment between the fault bends dips gently to the southeast (Figs 15a–c). On other parts of the Brazos fault, the segment between the fault bends is nearly horizontal (Fig. 15d). The hanging wall deformation closely resembles the deformation in the geometric models with the ramp-flat-ramp geometry (Figs 4g, 5b, 7 and 8d). Near the fault, growth beds dip toward the fault. Farther from the fault, growth beds dip gently away from the fault. A panel of dipping growth beds develops directly above the lower ramp. The geometry of the extensional fault-bend fold varies depending on the dip of the central segment. Where the segment is flat

(Fig. 15d), the growth beds directly above the panel of dipping growth beds are very thin. In fact, Vogler and Robinson (1987) report that a dipping unconformity locally overlies the panel of dipping growth beds. Where the segment is dipping (Fig. 15c), the growth beds directly above the panel of dipping growth beds are slightly thicker. The abrupt change in the style of the fault-bend folding with depth (i.e., tight folding at depth; broad folding at shallow levels) probably reflects significant aggradation during the latter stages of faulting and folding (Fig. 8d).

The low-angle, east-dipping Vicksburg fault underlies the Slick Ranch field in southern Texas (Fig. 16) (Erxleben & Carnahan 1983). The deformation in the hanging wall of the Vicksburg fault resembles that in the hanging

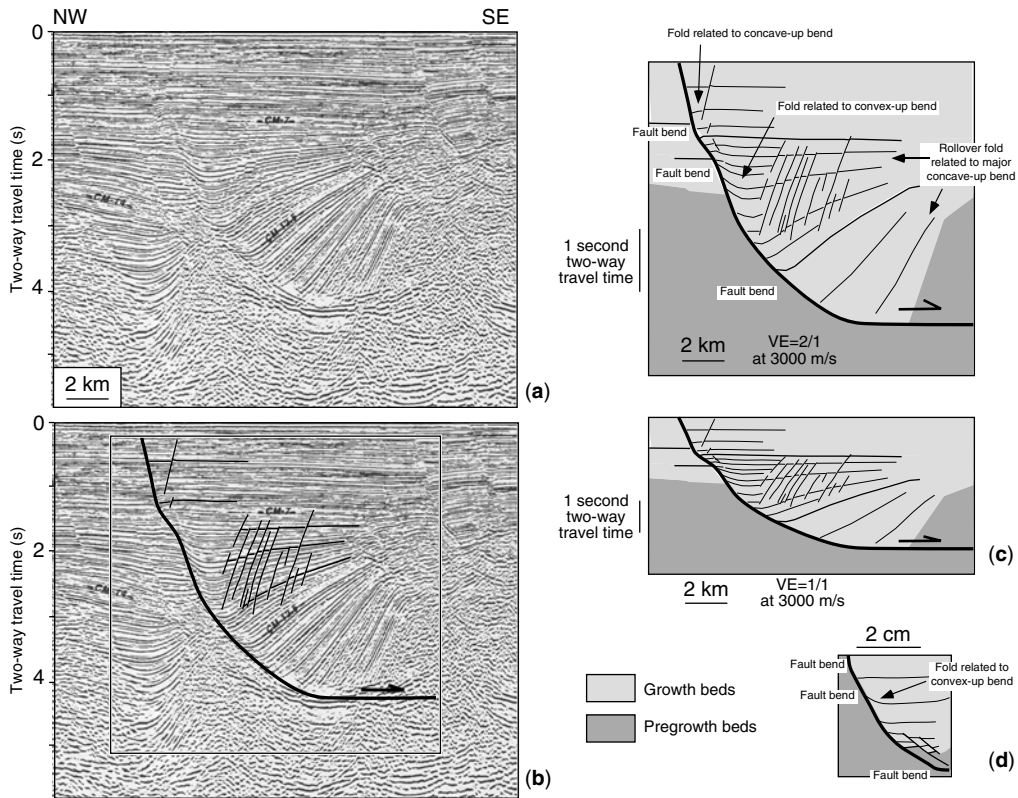


**Fig. 14.** Blackberry normal fault, offshore Texas, Gulf of Mexico. (a) Time-migrated seismic line (after Bally *et al.* 1991). CM-7 and CM-12.5 represent strata that are about 7 Ma and 12.5 Ma, respectively. (b) Interpreted seismic data. Black box shows location of line drawing. (c) Interpreted line drawing with (top) and without (bottom) vertical exaggeration. Second-order fault-bend folding occurs near small fault bends. (d) Second-order fault-bend fold in clay model with overlapping metal plates and 6 cm displacement.

wall of the Brazos fault in terms of geometry and dimensions (Fig. 15e). A panel of dipping growth beds overlies the low-angle fault. A dipping unconformity overlies the panel of dipping growth beds. As in the case of the Brazos fault, this deformation probably reflects movement on a fault with a ramp-flat-ramp geometry.

**Conclusions**

We have used geometric and experimental models to better understand the development of extensional fault-bend folds. The geometric models show that:

(1) The shape of a normal fault controls the distribution of growth beds, the magnitude and direction of dip of the pre-growth and growth beds, the outer limit of folding in the pre-growth and growth beds, and the level of hanging wall

beds relative to their footwall counterparts (Fig. 4).

(2) If a fault has two planar segments, then fault displacement controls the distribution, but not the dip, of the deformed pre-growth and growth beds (Fig. 2b). If a fault has a curved segment, then fault displacement controls the dip, thickness, and distribution of the deformed pre-growth and growth beds (Fig. 5).

(3) Aggradation and erosion control the distribution of growth beds, the dip of the pre-growth and growth beds, and the outer limit of folding in the pre-growth and growth beds (Figs 6 and 7). The outer limit of the folding in the growth beds parallels the lower fault segment, if no aggradation or erosion occur (Fig. 5). With aggradation, the outer limit of the folding dips more steeply than the lower fault segment. With erosion, the outer limit of the folding dips more gently than the lower fault segment.

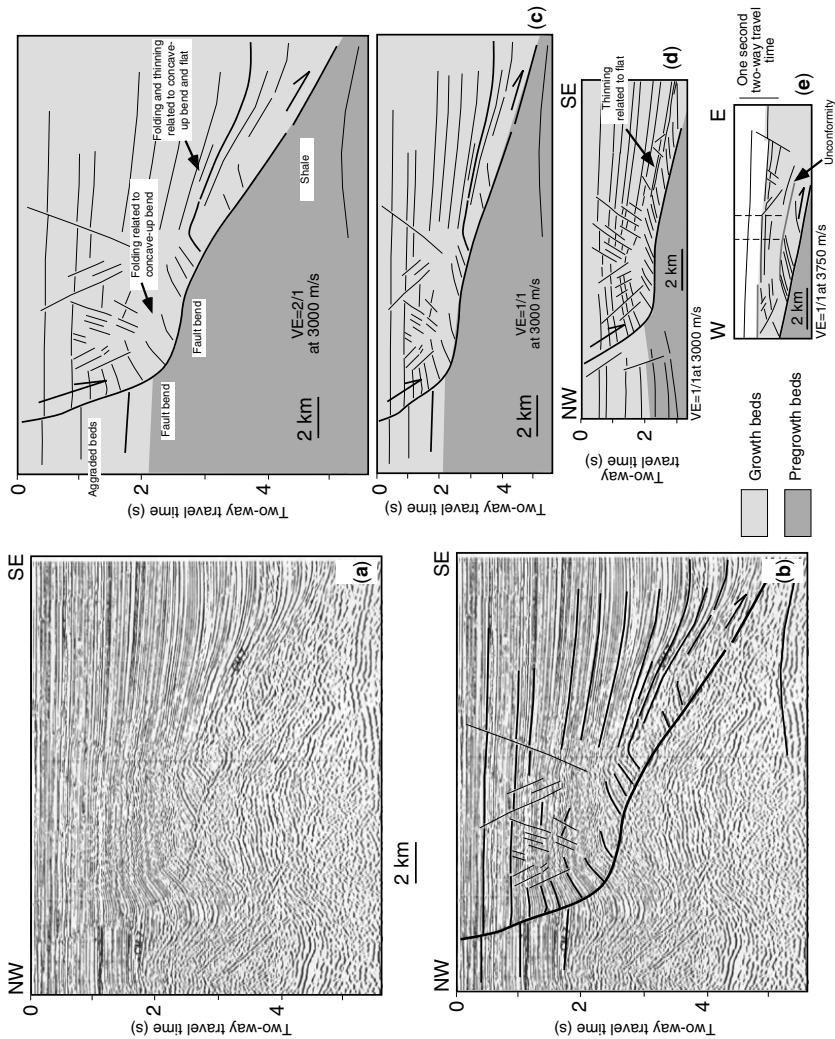


**Fig. 15.** (a) Time-migrated seismic line of Brazos fault, offshore Texas, Gulf of Mexico (after Bally *et al.* 1991). CM-7 represents strata that are about 7 Ma. (b) Interpreted seismic data. (c) Interpreted line drawing with (top) and without (bottom) vertical exaggeration. This part of the Brazos fault has two major fault bends. The intervening fault segment dips gently to the southeast. Beds near the fault dip toward the fault. Beds slightly farther from the fault. Antithetic and synthetic normal faults affect the hanging wall. (d) Interpreted line drawing of seismic line from different part of the Brazos fault. This part also has two major fault bends. The intervening fault segment is flat-lying. (e) Vicksburg fault near Slick Ranch field, southern Texas. Hanging wall deformation resembles that of Brazos fault in terms of geometry and dimension. Vertical dashed lines show well locations. See also Fig. 16.

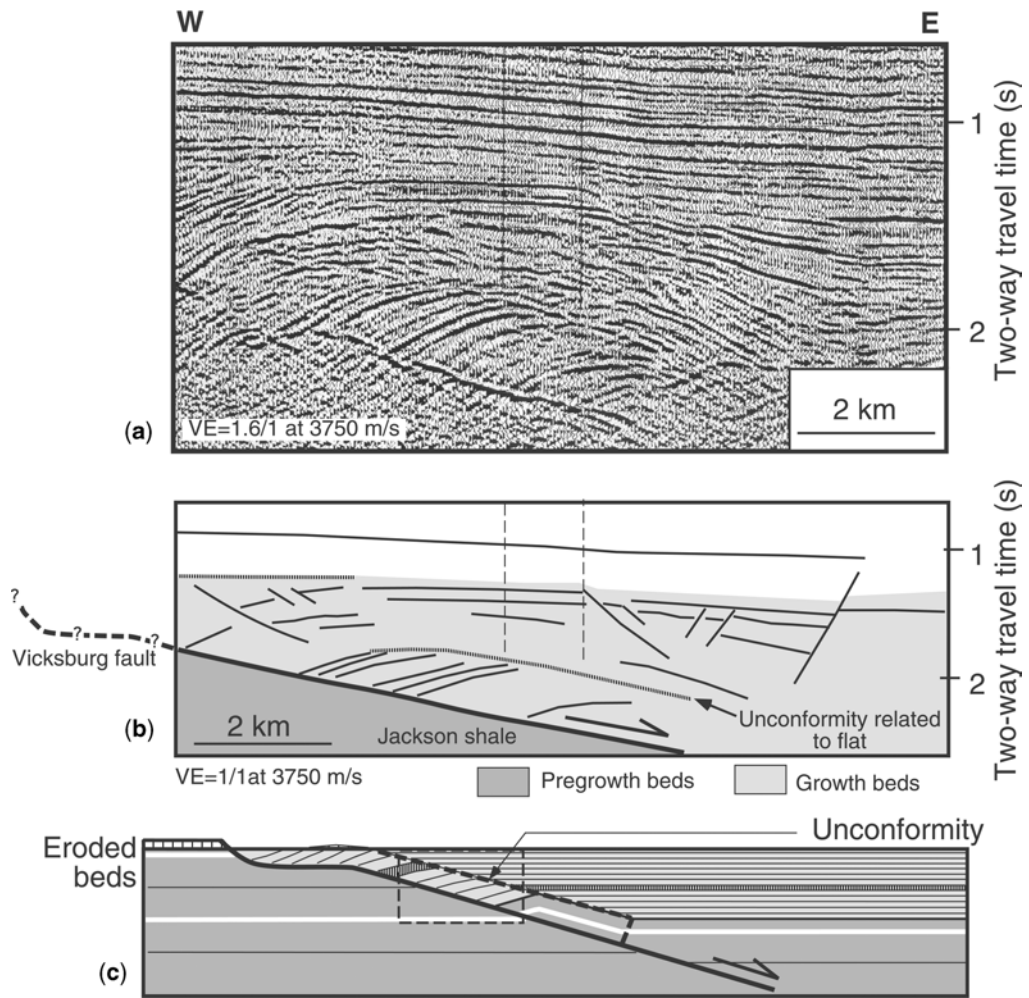


**Fig. 16.** Vicksburg fault near Slick Ranch field, southern Texas. Vertical dashed lines show well locations. (a) Uninterpreted seismic line with vertical exaggeration (after Erxleben & Carnahan 1983). (b) Interpreted line drawing of time-migrated seismic line displayed with approximately no vertical exaggeration (after Erxleben & Carnahan 1983). An unconformity separates a lower panel of growth beds dipping toward the fault from an upper panel dipping away from the fault. (c) Geometric model of ramp-flat-ramp fault showing unconformity similar to that in (b).

(4) Complex structural and stratigraphic patterns develop with multiple episodes of normal faulting if the rate of aggradation/erosion relative to the rate of fault displacement changes through time (Fig. 8). The outer limit of the folding dips more gently for growth packages associated with episodes of normal faulting without aggradation and more steeply for growth packages associated with episodes of normal faulting with aggradation. If erosion occurs between episodes of normal faulting, then growth beds associated with the first faulting episode can have a subtle fanning geometry and closely resemble pregrowth beds.

The experimental models indicate that the style of hanging wall deformation can vary considerably.

(1) In sand models, a few, relatively large secondary antithetic normal faults accommodate most hanging wall deformation. Pregrowth layers, although faulted, remain flat. The effective shear direction parallels the antithetic normal faults, and the shear angle is about 60°–65°.

(2) In clay models, secondary faulting (antithetic and synthetic) and cataclastic flow accommodate most of the hanging wall deformation. The deformed pregrowth and growth layers dip gently toward the main normal fault. The

effective shear angle ( $35^{\circ}$ – $50^{\circ}$ ) is considerably less than the dip of the antithetic normal faults.

(3) The sand and clay models resemble geometric models with large (*c.*  $60^{\circ}$ ) and small (*c.*  $35^{\circ}$ ) shear angles, respectively. In the sand models and the geometric models with large shear angles, more displacement occurs on the main normal fault and the hanging wall collapses in a relatively narrow zone. In the clay models and the geometric models with small shear angles, less displacement occurs on the main normal fault. Instead, the hanging wall stretches substantially and collapses in a relatively wide zone.

Observed hanging wall folds in nature resemble those in the geometric and experimental models. Rollover folds develop in the hanging wall of normal faults that flatten at depth. Normal faults with convex-up bends have hanging wall beds that dip away from the main fault. Normal faults with ramp-flat-ramp geometries have complex hanging wall deformation; beds dip toward the fault near the main fault, and a dipping unconformity that parallels the lower ramp commonly develops above the ramp. Observed secondary normal faults in nature resemble those in the experimental models, especially the clay models. Many secondary normal faults are antithetic to the main fault, but some are synthetic to the main normal fault. Most secondary normal faults have relatively small displacements.

### Appendix: scaling

The strength of most upper crustal rocks increases with depth, obeying a Mohr-Coulomb criterion of failure (e.g., Byerlee 1978). According to this criterion,

$$\tau = c + \mu \cdot \sigma_n, \quad (1)$$

where  $\tau$  and  $\sigma_n$  are, respectively, the shear and normal stresses on a potential fault surface,  $c$  is the cohesion, and  $\mu$  is the coefficient of internal friction. This empirical criterion of failure describes the initiation of new faults rather than the frictional reactivation of existing faults. For most sedimentary rocks,  $\mu$  ranges from about 0.55–0.85 (e.g., Handin 1966; Byerlee 1978). For intact sedimentary rocks,  $c$  is about 10–20 MPa (Handin 1966), whereas for highly fractured sedimentary rocks,  $c$  is significantly less (e.g., Byerlee 1978; Brace & Kohlstedt 1980). To ensure dynamic similarity between the models and natural prototypes, two conditions must be satisfied (e.g., Hubbert 1937; Weijermars *et al.* 1993; Vendeville *et al.* 1995).

First, the modelling materials and the rocks in nature must have similar coefficients of internal friction. This condition is satisfied with either dry sand or wet clay as the modelling material. Second,

$$c^* = \rho^* \cdot g^* \cdot l^*, \quad (2)$$

where  $c^*$ ,  $\rho^*$ ,  $g^*$  and  $l^*$  are model-to-natural prototype ratios for cohesion, density, gravity and length, respectively. In our models, the values of  $\rho^*$  and  $g^*$  are about 0.7 and 1, respectively, and  $l^*$  is about  $10^{-5}$  (i.e., 1 cm in the models equals about 1 km in nature). Thus, to ensure dynamic similarity between the models and natural prototypes, the cohesion of rock must be about  $10^5$  greater than that of the modelling materials. This condition is satisfied with either dry sand or wet clay as the modelling material.

We thank E. Peterson for his assistance with the geometric modelling, and S. Callaway, S. Dixon, G. Eisenstadt and D. Sims for their help with the experimental models. We also wish to thank G. Corti, T. Dooley and B. Vendeville for their helpful reviews of the manuscript. The research was partially supported by NSF grant EAR-0408878.

### References

- BALLY, A., WITHJACK, M., MEISLING, K. & FISHER, D. 1991. *Seismic expression of structural styles*. Geological Society of America, Short Course Notes, 1991 National Meeting.
- BRACE, W. F. & KOHLSTEDT, D. L. 1980. Limits on lithospheric stress imposed by laboratory experiments. *Journal of Geophysical Research*, **85**, 6248–6252.
- BYERLEE, J. 1978. Friction of rocks. *Pure Applied Geophysics*, **116**, 615–626.
- CLOOS, E. 1968. Experimental analysis of Gulf Coast fracture patterns. *American Association of Petroleum Geologists Bulletin*, **52**, 420–444.
- CLOOS, H. 1928. Experimente zur inneren tektonik. *Zentralblatt für Mineralogie*, **B**, 609–621.
- CLOOS, H. 1930. Kunstliche gebirge, II. *Natur und Museum*, **60**, 258–269.
- DULA, W. F. 1991. Geometric models of listric normal faults and rollover folds. *American Association of Petroleum Geologists Bulletin*, **75**, 1609–1625.
- ELLIS, P. G. & McCLAY, K. R. 1988. Listric extensional fault systems – results of analogue model experiments. *Journal of Basin Research*, **1**, 55–70.
- ERXLEBEN, A. W. & CARNAHAN, G. 1983. Slick Ranch area, Starr County, Texas. In: BALLY, A. W. (ed.) *Seismic Expression of Structural Styles*. American Association of Petroleum Geologists, Studies in Geology, **15**, 2.3.1, 22–26.

- HANDIN, J. 1966. Strength and ductility. In: CLARK, S. P. Jr. (ed.) *Handbook of Physical Constants*. Geological Society of America, **Memoir 97**, 223–289.
- HAUGE, T. A. & GRAY, G. G. 1996. A critique of techniques for modelling normal-fault and rollover geometries. In: BUCHANAN, P. G. & NIEUWLAND, D. A. (eds) *Modern Developments in Structural Interpretation, Validation and Modelling*. Geological Society, London, Special Publications, **99**, 89–97.
- HUBBERT, M. K. 1937. Theory of scale models as applied to the study of geologic structures. *Geological Society of America Bulletin*, **48**, 1459–1520.
- KAUTZ, S. A. & SCLATER, J. G. 1988. Internal deformation in clay models of extension by block faulting. *Tectonics*, **7**, 823–832.
- KERR, H. G. & WHITE, N. 1992. Laboratory testing of an automatic method for determining normal fault geometry at depth. *Journal of Structural Geology*, **14**, 873–885.
- MCCLAY, K. R. & ELLIS, P. G. 1987a. Analogue models of extensional fault geometries. In: COWARD, M. P., DEWEY, J. F. & HANCOCK, P. L. (eds) *Continental Extensional Tectonics*. Geological Society, London, Special Publications, **28**, 109–125.
- MCCLAY, K. R. & ELLIS, P. G. 1987b. Geometries of extensional fault systems developed in model experiments. *Geology*, **15**, 341–344.
- MCCLAY, K. R. & SCOTT, A. D. 1991. Experimental models of hangingwall deformation in ramp-flat listric extensional fault systems. *Tectonophysics*, **188**, 85–96.
- RUTTER, E. H. 1986. On the nomenclature of mode of failure transition in rocks. *Tectonophysics*, **122**, 381–387.
- VENDEVILLE, B., HONGXING, G. & JACKSON, M. P. A. 1995. Scale models of salt tectonics during basement-involved extension. *Petroleum Geoscience*, **1**, 179–183.
- VOGLER, H. A. & ROBINSON, B. A. 1987. Exploration for deep geopressured gas—Corsair trend, offshore Texas. *American Association of Petroleum Geologists Bulletin*, **71**, 777–787.
- WEIJERMARS, R., JACKSON, M. P. A. & VENDEVILLE, B. 1993. Rheological and tectonic modeling of salt provinces. *Tectonophysics*, **217**, 143–174.
- WERNICKE, B. P. & BURCHFIELD, B. C. 1982. Modes of extensional tectonics. *Journal of Structural Geology*, **4**, 105–115.
- WHITE, N. 1992. A method for automatically determining normal fault geometry at depth. *Journal of Geophysical Research*, **97**, 1715–1733.
- WHITE, N. J. & YIELDING, G. 1991. Calculating normal fault geometries at depth: theory and examples. In: ROBERTS, A. M., YIELDING, G. & FREEMAN, B. (eds) *The Geometry of Normal Faults*. Geological Society, London, Special Publications, **56**, 251–260.
- WHITE, N. J., JACKSON, J. A. & MCKENZIE, D. P. 1986. The relationship between the geometry of normal faults and that of the sedimentary layers in their hanging walls. *Journal of Structural Geology*, **8**, 897–909.
- WITHJACK, M. O. & CALLAWAY, J. S. 2000. Active normal faulting beneath a salt layer – an experimental study of deformation in the cover sequence. *American Association of Petroleum Geologists Bulletin*, **84**, 627–651.
- WITHJACK, M. O. & PETERSON, E. T. 1993. Prediction of normal-fault geometries – a sensitivity analysis. *American Association of Petroleum Geologists Bulletin*, **77**, 1860–1873.
- WITHJACK, M. O., ISLAM, Q. & LAPOINTE, P. 1995. Normal faults and their hanging-wall deformation – an experimental study. *American Association of Petroleum Geologists Bulletin*, **79**, 1–18.
- XIAO, H. & SUPPE, J. 1992. Origin of rollover. *American Association of Petroleum Geologists Bulletin*, **76**, 509–529.
- YIELDING, G., BADLEY, M. E. & FREEMAN, B., 1991. Seismic reflections from normal faults in the northern North Sea. In: ROBERTS, A. M., YIELDING, G. & FREEMAN, B. (eds) *The Geometry of Normal Faults*. Geological Society, London, Special Publications, **56**, 79–89.

